Pergamon

0956-7151(95)00163-8

Acta mater. Vol. 44, No. 1, pp. 315–325, 1996
Elsevier Science Ltd

1359-6454/96 $15.00 + 0.00

MODELLING DAMAGE OF Al–Zn–Mg ALLOYS

R. LEBENSOHN†[1], D. SOLAS[1], G. CANOVA[1] and Y. BRECHET[2]

[1]GPM2, ENSPG and [2]LTPCM, ENSEEG, Domaine Universitaire, 38402 St. Martin d'Heres Cedex, France

(Received 23 January 1995; in revised form 3 March 1995)

Abstract—The present work is concerned with the modelling of damage initiation and growth in Al–Zn–Mg alloys, and also with an estimation of the ductility in uniaxial tension. An elastoplastic self-consistent model is developed accounting for crystallographic texture and grain shape effects, which also integrates the voids formed by the damage process. The damage evolution is followed within this framework, allowing the prediction of the macroscopic mechanical behavior, and particularly the stress–strain curves for different tensile directions. A bifurcation analysis adapted for this anisotropic compressible case was developed and used to estimate the ductility. Effects of texture, grain shape and critical parameters for damage nucleation are investigated on a theoretical basis. The observed yield stress and fracture strain vs tensile angle profiles observed experimentally can be predicted for certain cases.

On présente, dans ce travail, une modélisation de la nucléation et croissance de l'endommagement dans les alliages Al–Zn–Mg, avec une estimation de la ductilité en traction. Un modèle autocohérent élastoplastique est développé, qui prend en compte les effets de texture et de forme des grains, et qui aussi intègre les cavités formées pendant le processus d'endommagement. L'evolution de l'endommagement est suivi dans ce contexte, permettant la prédiction du comportement mécanique, et particulièrement les courbes contrainte/déformation dans différentes directions. Une analyse de bifurcation adaptée pour ce cas anisotrope compressible a été développée et utilisée pour estimer la ductilité. Les effets de texture, forme des grains et des paramètres critiques de nucléation sont étudiés sur une base théorique. Les profils de limites élastiques et de déformation à rupture en fonction de l'angle de sollicitation peuvent être prédits dans certains cas.

1. INTRODUCTION

Modelling anisotropy of mechanical properties is a long standing problem of mechanical metallurgy. It is of special practical importance for alloys with high performances such as the 7000 series used in the aeronautical industry. If anisotropy of yield stress has been extensively studied [1], the problem of damage has been comparatively less investigated. Indeed, most of the studies concerning the micromechanisms of damage and their relation with fracture properties have overlooked the question of anisotropy [2, 3]. The purpose of this paper is to show, on the special case of Al–Zn–Mg alloys for which the fracture mechanisms have been well identified, a method which allows damage growth in a polycrystalline plasticity scheme in order to describe the anisotropy of mechanical properties, including the ductility.

The Al–Zn–Mg alloys form the basis of the 7000 series and can be used as model alloys for a study of damage anisotropy. The damage mechanisms have been thoroughly studied and the resulting fracture morphologies are well understood [4]. The aspects of microstructure relevant to damage properties are well known. This alloy is the prototype alloy associated with the phenomenon of ductile intergranular failure [5]. Therefore most of the damage events take place at the grain boundaries, either by shear failure or by decohesion. This relative simplicity of the system allows us to derive a model including texture and damage. Furthermore, measurements of yield stress and ductility of tensile samples cut at different angles from an Al–Zn–Mg sheet are available [4]. Figure 1 shows typical profiles of yield stress and ductility (i.e. maximum tensile strain) as a function of the angle formed by the tensile axis and the rolling direction (RD) of the sheet. All the samples were cut normal to the transverse direction (TD) of the sheet. The orientations of the samples in the RD–ND plane (ND: normal direction) are designed as: "L" (along RD), "TB45" and "TB60" (at 45° and 60° from RD, respectively) and "TC" (along ND). The mean features in these profiles are:

(a) the yield stress for the L sample is higher than for the other orientations;
(b) the ductility profile shows a minimum for the TB orientations.

In this contribution, we do not attempt to fill the gap between the microstructure characteristics (such as the width of the precipitate free zones at the grain

†Permanent address: Instituto de Fsica Rosario (UNR-CONICET), 27 Febrero 210 bis, 2000 Rosario, Argentina.

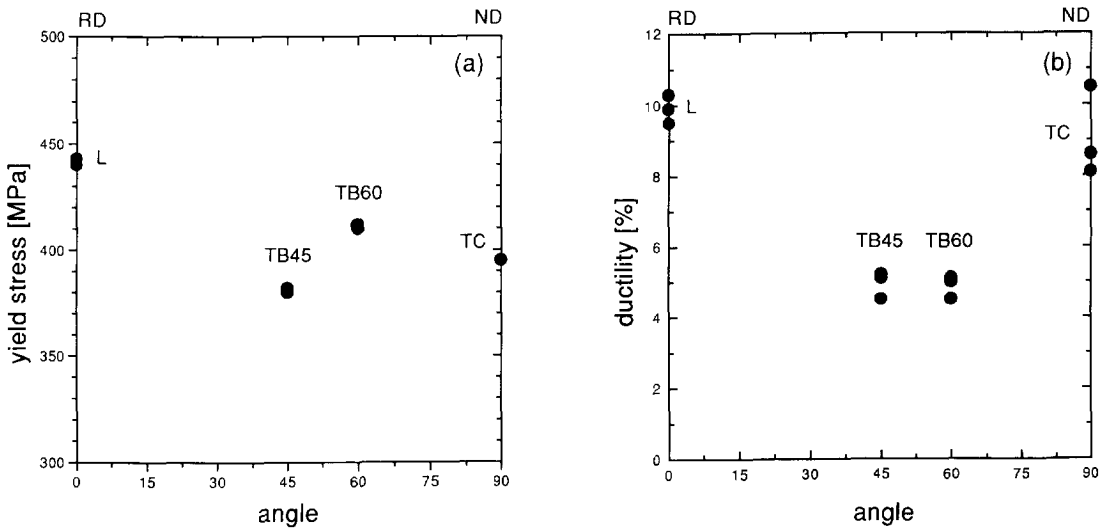

Fig. 1. Yield stress and ductility of tensile samples cut from an Al–Zn–Mg sheet for different orientations of the tensile axis in the RD–ND plane (after Solas *et al.* [4]).

boundary) and the macroscopic properties (as ductility). We rather make use of our knowledge of the damage mechanisms to implement local phenomenological damage criteria at the mesoscopic level into a self-consistent elastoplastic model.

The paper is structured as follows: in Section 2 we summarize the experimental observations at the mesoscopic level which allows one to identify the dominant damage mechanisms and the relevant criteria for nucleation of damage. In Section 3 the elastoplastic model including the above damage criteria is presented and a condition for general failure based on a bifurcation analysis is given. The influence of the various input parameters is investigated and discussed in Sections 4 and 5, respectively.

2. MICROSTRUCTURAL ASPECTS OF DAMAGE

The purpose of this section is not to give an exhaustive description of the microstructure of the Al–Zn–Mg alloy we consider, which can be found elsewhere [4]. It is just intended to describe the salient features which justify the form of the damage criteria that has been used in the model presented in Section 3.

A general feature of the 7000 series is the existence of a precipitate free zone near grain boundaries. The precipitates being responsible for the high yield stress of those alloys, there exists therefore close to the grain boundary a "soft zone" in which plastic flow tends to localize. As the grain boundaries are decorated by coarse precipitates, this intense plastic flow leads to void nucleation at the particles, and then to void growth and ultimately to the failure of the grain boundary. This failure can occur either in shear or in tension depending on the dominant solicitation of the grain boundary. As a consequence, the main damage process in this type of alloy is ductile intergranular failure [5]. The resulting fracture morphology is mainly intergranular, except for some intragranular shear failure probably associated with the final fracture event. The overall fracture surface for a given straining direction reflects the competition between the imposed maximum shear direction and the microstructural anisotropy.

The salient features from those observations, relevant to our purpose, are summarized as follows:

(a) the damage events nucleate at grain boundaries;
(b) grain boundaries can fail either in shear or tension. They are weaker in shear due to the presence of precipitate free zones of limited width [4];
(c) the final brutal failure can follow paths either inside the grains or along grain boundaries.

In order to implement this information in the model presented in the next section, the various scales involved in the description must be clearly identified. At the mesoscopic scale, the damage mechanisms are nucleation and growth of voids at the particles along the grain boundary surrounded by a precipitate free zone. This mechanism has been successfully modelled for shear failure by Embury and Nes [3]: it leads to a criterion for the shear failure of the grain boundary expressed by a critical strain. For the tensile failure of the grain boundary with precipitates and a precipitate free zone, no model is presently available, but the classical work on ductile failure [3] can be adapted. It would lead to a critical normal strain, which for the tensile geometry corresponds to a critical normal stress. At the mesoscopic scale, a grain boundary will fail under tension when a critical normal stress is reached, and in shear when the critical shear strain is attained. Those are the criteria for damage at the mesoscopic scale which have to be introduced in an elastoplastic self-consistent scheme in order to incorporate damage. As the final failure is both

inter- and transgranular whereas the main damage mechanisms were intergranular damage, it is likely that the final ruin will occur by an overall mechanical instability of the system. This suggests that the macroscopic criterion for final fracture has to be an instability criterion at the continuum level.

From those qualitative observations on the failure mechanisms, we can therefore deduce the appropriate form of the mesoscopic damage nucleation (failure of a grain boundary) either in shear or in tension. The numerical values of those phenomenological criteria are not derived here from the underlying microstructure (width of a preciptate free zone, size and spacing of the coarse precipitates, yield stress of the grain interior). They are introduced in the model as the reasonable form of criteria for mesoscopic damage for this kind of alloy.

3. MODELLING

Different approaches are required to have a reliable description of the mechanical behavior of a polycrystalline aggregate containing cavities. To start with, the elastoplastic response of a polycrystal in its initial, undamaged state is obtained by means of the elastoplastic self-consistent (EPSC) model [6, 7]. If the single crystal constitutive equation, the orientations distribution and the grain morphology are known, the EPSC model gives the instantaneous micro and macro relationships between stress rates and strain rates. Therefore, using EPSC along incremental time steps, it is possible to compute whether certain critical conditions for nucleation of intergranular cavities are reached. When some cavities appear inside the material, the polycrystal becomes a "composite" with two populations of "particles": grains and voids (voids are considered particles having zero stiffness). Hence, the EPSC model must be extended to consider the case of such a composite material. Since voids are "soft" particles compared to grains, the local strain rate is greater for voids than for grains and a gradual increase of the relative volume of voids is expected. Furthermore, the appearance of voids modifies the instantaneous macroscopic behavior of the polycrystal.

This micro–macro description of the mechanical behavior of a damaged elastoplastic polycrystal can be linked to a pure macroscopic criterion to estimate the ductility of the material. Assuming that the final stage of damage leading to fracture occurs soon after the initiation of the unstable plastic flow, we can use the instantaneous macroscopic state (calculated with the EPSC model) to determine whether the plastic instability condition is reached. The instability analysis is performed applying the bifurcation theory [8–11] to the case of a compressible anisotropic material under plane-strain conditions.

The present modelling is formulated in a small strain framework for different reasons. Firstly, the material to be analyzed has, in general, a very sharp texture, that can be assumed to remain invariant after subsequent testing. Next, the ductility of such materials is sufficiently small after heavy cold rolling to justify the use of small strain formalism.

3.1. The elastoplastic self-consistent formulation

The initial polycrystal is described by means of a set of orientations with associated weights. Each orientation represents a grain and its weight corresponds to the relative volume of the grain with respect to the entire polycrystal. The actual distribution of orientations and weights depends on the polycrystal's crystallographic texture. A given shape is assigned to each grain (for simplicity, an ellipsoidal shape for every grain can be assumed). When a stress or strain increment is imposed to the polycrystal in a given time step, the strain–stress increment in each grain as well as the macroscopic behavior is calculated using the Hill–Hutchinson elastoplastic self-consistent (EPSC) formulation [6, 7]. The EPSC model is a one-site formulation based on Eshelby's solution of the inclusion problem [12]. Within EPSC, each grain is considered as an elastoplastic inclusion deforming inside an elastoplastic homogeneous equivalent medium (HEM). This HEM has the average (macroscopic) properties of the polycrystal. At the microscopic level, the grain behaves according to the following constitutive relation

$$\dot{\boldsymbol{\sigma}} = \mathbf{C}^{g}:(\dot{\epsilon} - \sum^{s} \mathbf{m}^{s}\dot{\gamma}^{s}) \tag{1}$$

where $\dot{\sigma}$ is the Cauchy stress rate, $\dot{\epsilon}$ is the total strain rate, $\mathbf{C}^{g}$ is the local elastic stiffness, $\mathbf{m}^{s}$ is the Schmid tensor of the slip system s defined as

$$m_{ij}^{s} = \tfrac{1}{2}(n_i^s b_j^s + n_j^s b_i^s) \tag{2}$$

($\mathbf{n}$ and $\mathbf{b}$ are the normal to the slip plane and Burgers vector of the slip system, respectively) and $\dot{\gamma}^{s}$ is the shear rate of the slip system s. The sum on s in equation (1) runs over all the active slip systems. Following Hutchinson [7], a given slip system s is considered as *potentially* active if

$$\mathbf{m}^{s}:\boldsymbol{\sigma} = \tau^{s} \tag{3}$$

where τ^{s} is the yield stress of the system s, but it will be considered as *actually* active only if the following relation between rates holds

$$\mathbf{m}^{s}:\dot{\boldsymbol{\sigma}} = \dot{\tau}^{s}. \tag{4}$$

The rate of change of the yield stress $\dot{\tau}^{s}$ is related to the shear rate through the microscopic hardening law

$$\dot{\tau}^{s} = \sum_{s'} h^{ss'}\dot{\gamma}^{s'} \tag{5}$$

where s and s' run over all the slip systems. Projecting both sides of equation (1) on the Schmid tensor and

using equations (4) and (5) the following relation can be obtained

$$\sum_{s'} (h^{ss'} + \mathbf{m}^s{:}\mathbf{C}^g{:}\mathbf{m}^{s'})\dot{\gamma}^{s'} = \mathbf{m}^s{:}\mathbf{C}^g{:}\dot{\boldsymbol{\epsilon}}. \tag{6}$$

If for given set of S active systems, it is possible to invert the $S \times S$ matrix $\mathbf{X}$ defined as

$$X^{ss'} = h^{ss'} + \mathbf{m}^s{:}\mathbf{C}^g{:}\mathbf{m}^{s'} \tag{7}$$

then, the following relation holds

$$\dot{\gamma}^s = \mathbf{f}^s{:}\dot{\boldsymbol{\epsilon}} \tag{8}$$

where

$$\mathbf{f}^s = \sum_{s'} (X^{ss'})^{-1}\mathbf{m}^{s'}{:}\mathbf{C}^g \tag{9}$$

is a second-rank tensor associated with each active system s. Using equations (8) and (9) in equation (1) we obtain the microscopic tangent elastoplastic stiffness $\mathbf{L}^g$

$$\dot{\sigma} = [\mathbf{C}^g{:}(\mathbf{I} - \sum^{s} \mathbf{m}^s \otimes \mathbf{f}^s)]{:}\dot{\epsilon} = \mathbf{L}^g{:}\dot{\boldsymbol{\epsilon}}. \tag{10}$$

At the macroscopic level, the polycrystal's stress rate $\dot{\boldsymbol{\Sigma}}$ and strain rate $\dot{\mathbf{E}}$ are linearly related through the macroscopic tangent elastoplastic stiffness $\mathbf{L}$

$$\dot{\boldsymbol{\Sigma}} = \mathbf{L}{:}\dot{\mathbf{E}}. \tag{11}$$

The *interaction equation* relates the deviations of the local magnitudes with respect to the macroscopic ones

$$\dot{\boldsymbol{\sigma}} - \dot{\boldsymbol{\Sigma}} = -\tilde{\mathbf{L}}{:}(\dot{\boldsymbol{\epsilon}} - \dot{\mathbf{E}}). \tag{12}$$

The *interaction tensor* $\tilde{\mathbf{L}}$ is given by the expression

$$\tilde{\mathbf{L}} = \mathbf{L}{:}(\mathbf{S}^{-1} - \mathbf{I}) \tag{13}$$

where the *elastoplastic Eshelby tensor* $\mathbf{S}$ is a function of the macroscopic elastoplastic stiffness $\mathbf{L}$ and the shape of the ellipsoid (the algorithm for the calculation of Eshelby tensor for a general ellipsoid and an arbitrary anisotropic medium can be found elsewhere [13]). Using equations (10)–(12), the microscopic and macroscopic strain rate can be related through the *localization tensor* $\mathbf{A}^g$

$$\dot{\boldsymbol{\epsilon}} = (\mathbf{L}^g + \tilde{\mathbf{L}})^{-1}{:}(\tilde{\mathbf{L}} + \mathbf{L}){:}\dot{\mathbf{E}} = \mathbf{A}^g{:}\dot{\mathbf{E}}. \tag{14}$$

Local and macroscopic magnitudes are linked through the following *micro–macro relations*

$$\langle \dot{\boldsymbol{\epsilon}} \rangle = \dot{\mathbf{E}} \tag{15}$$

$$\langle \dot{\boldsymbol{\sigma}} \rangle = \dot{\boldsymbol{\Sigma}} \tag{16}$$

where $\langle\ \rangle$ denotes volume average. Taking the volume average of equation (14) and using equation (15) leads to

$$\langle \mathbf{A}^g \rangle = \mathbf{I}. \tag{17}$$

Furthermore, using equations (10), (16) and (11), we obtain the following *self-consistent equation*

$$\mathbf{L} = \langle \mathbf{L}^g{:}\mathbf{A}^g \rangle. \tag{18}$$

Let us assume that the grain morphology and the texture of an elastoplastic polycrystal are known (e.g. $\mathbf{C}^g$ and $\mathbf{m}^s$ can be determined for each grain). Furthermore, the current local stresses $\boldsymbol{\sigma}$ (e.g. the potentially active systems) of every grain and the current macroscopic modulus $\mathbf{L}$ are known, as well. If a macroscopic stress rate $\dot{\boldsymbol{\Sigma}}$ is imposed on the polycrystal in a given time step Δt, the values of the microscopic and macroscopic moduli can be updated using the following scheme. Making a guess for the macroscopic modulus $\mathbf{L}$, we calculate the Eshelby tensor $\mathbf{S}$, the interaction tensor $\tilde{\mathbf{L}}$ and the macroscopic strain rate $\dot{\mathbf{E}}$. With another guess—made on the set of actually active systems—and using equations (7), (9) and (10), we calculate the tensors $\mathbf{f}^s$ and the microscopic moduli $\mathbf{L}^g$ for each grain. Using equation (14), with $\mathbf{L}^g$, $\mathbf{S}$ and $\tilde{\mathbf{L}}$ we get $\mathbf{A}^g$, and knowing $\dot{\mathbf{E}}$, we obtain the local strain rate $\dot{\boldsymbol{\epsilon}}$. Next, the microscopic shear rates $\dot{\gamma}^s$ [equation (8)] and the local stress rate $\dot{\boldsymbol{\sigma}}$ [equation (10)] are calculated. With $\dot{\boldsymbol{\sigma}}$, and getting the rate of change of the critical stress $\dot{\tau}^s$ through the microscopic hardening law [equation (5)] we can check if the condition (4) is satisfied (if this is not the case, a new guess for the set of actually active systems must be made). Next, the self-consistent relation equation (18) is used for improving the guess for the macroscopic modulus $\mathbf{L}$. Convergence is reached if the average $\langle \mathbf{L}^g{:}\mathbf{A}^g \rangle$ coincides with the input value of $\mathbf{L}$ within a certain tolerance. Finally, assuming that rates are constant along Δt, the current micro and macro stress and strain are updated and a new time step is applied to the polycrystal.

It must be mentioned (as stated by Hutchinson [7]) that the microscopic modulus $\mathbf{L}^g$ is unique, even if the set of shear rates is not. This non-uniqueness of $\dot{\gamma}^s$ is irrelevant whereas our approach remains within *small strain formulation* (e.g. crystal rotation due to slip activity is not taken into account). It means, in particular, that, assuming isotropic hardening of the slip systems, the sum of the shear rates over the active systems is also unique, which induces a uniquely defined variation of the critical stresses. The ambiguity in the slip systems choice would lead to non-uniquity concerning the grain reorientation, which is not considered here. It is therefore necessary to find out only one possible set of actually active systems to determine the instantaneous response of the grain.

If some (ellipsoidal) voids appear inside the polycrystal, they get into the same scheme as new "particles" having $\mathbf{L}^g = 0$. The localization tensor for voids is

$$\mathbf{A}^g = \mathbf{I} + \tilde{\mathbf{L}}^{-1}{:}\mathbf{L}. \tag{19}$$

If the shape of the voids (e.g. aspect ratio and orientation of principal axes of the ellipsoid) differs

from the grain shape, both the Eshelby tensor $\mathbf{S}$ and the interaction tensor $\tilde{\mathbf{L}}$ are going to be different for both population of "particles". Therefore, it is evident from equation (12) that the simultaneous fulfillment of the micro–macro relations of equations (15) and (16) is not guaranteed in advance. Different numerical procedures were proposed to overcome this problem [14, 15]. Accordingly, we assume that the local strain rate is localized with respect to an *a priori* unknown reference strain rate $\dot{\mathbf{E}}^*$

$$\dot{\epsilon} = \mathbf{A}^g : \dot{\mathbf{E}}^*. \tag{20}$$

Hence

$$\dot{\mathbf{E}} = \langle \mathbf{A}^g \rangle : \dot{\mathbf{E}}^*. \tag{21}$$

Using equation (20) [instead of equations (14) and (21)] within the same scheme described earlier, we obtain an extended self-consistent relation [14]

$$\mathbf{L} = \langle \mathbf{L}^g : \mathbf{A}^g \rangle : \langle \mathbf{A}^g \rangle^{-1}. \tag{22}$$

It is evident that when all the particles inside the polycrystal have the same shape [e.g. equation (17) holds], equation (22) reduces to the original self-consistent equation (18).

Unlike grains, and provided the distortion of voids can be very high, rotations of cavities must be considered. The expression for local rotation rates is

$$\dot{\omega} = \mathbf{\Pi} : \mathbf{S}^{-1} : \dot{\epsilon} \tag{23}$$

where $\mathbf{\Pi}$ is the antisymmetric Eshelby rotation tensor [16]. After each time step, the relative weights w^g of grains and voids are updated taking into account the local volume change

$$w^{g(\text{new})} = [1 + \text{tr}(\dot{\epsilon})\Delta t] w^{g(\text{old})}. \tag{24}$$

In this way, the total volume fraction of voids increases after each time step.

3.2. *Bifurcation theory*

In this analysis, it is assumed that the tensile specimen exhibits a homogeneous state of stress and strain rates. At a given moment, the material has reached a given state characterized by a homogeneous macroscopic tangent tensor $\mathbf{L}$. It is assumed that an instability, if any, will occur in the form of a band, inclined at a certain angle with respect to the tensile direction. A perturbation in the stress rate/strain rate fields is introduced that must fulfill both equilibrium and compatibility relations of the band with the bulk. The question is to know whether the perturbation can survive or not, i.e. be non-zero. If such is the case, the instability will be considered to lead to fracture in a short amount of time, so that the bifurcation strain will be identified to the ductility.

The next development follows the guidelines due to Stören and Rice [10], Hutchinson and Neale [11], and Canova *et al.* [17]. If $\mathbf{n}$ defines the unit vector orthogonal to the groove, the jumps in the velocity field are expected of the form

$$\Delta v_i = f_i(X_n = \mathbf{X} \cdot \mathbf{n}) \tag{25}$$

where the vector $\mathbf{X}$ represents the position of a point of the sample in tensile axes (X_3 being along the tensile direction) and X_n its component along $\mathbf{n}$. A jump in the velocity gradient will be written as

$$\Delta v_{i,j} = \frac{\partial \Delta v_i}{\partial X_j} = g_i n_j \tag{26}$$

where

$$g_i = \frac{\partial f_i}{\partial X_n}. \tag{27}$$

The equilibrium condition can be expressed by the equation

$$\Delta \dot{T}_j = n_i \Delta t_{ij} = 0 \tag{28}$$

where $\dot{\mathbf{T}}$ is the nominal force rate and t_{ij} the nominal stress rate defined by

$$t_{ij} = \dot{\sigma}_{ij} - v_{i,k}\sigma_{kj} + \sigma_{ij}\,\text{tr}(\dot{\epsilon}) \tag{29}$$

in which the rate of Cauchy stress $\dot{\sigma}$ is obtained by means of the self-consistent procedure. Equations (28) and (29) lead to the following system

$$\begin{vmatrix} A \times g_1 + B \times g_3 = 0 \\ C \times g_1 + D \times g_3 = 0 \end{vmatrix} \tag{30}$$

where the 2×2 matrix built up with A, B, C and D depends on the state of the material, i.e. its stress $\boldsymbol{\sigma}$ and its tangent properties expressed in the tensor $\mathbf{L}$, and on the groove angle, known through $\mathbf{n}$. The detailed way of calculating A, B, C and D is exposed in the Appendix. It is enough to test, for each iterative state of the material, and for each groove angle, if the matrix has a zero determinant for bifurcation to occur, giving therefore an estimate of the material ductility.

4. RESULTS

The influence of texture, grain shape and microstructure (the latter, through the critical conditions for void nucleation) on the elastoplastic behavior of a damaged polycrystal was investigated using the EPSC model plus the corresponding bifurcation analysis. Tensile tests on samples cut out from a sheet along different directions in the RD–ND (rolling direction–normal direction) plane were simulated setting different input parameters. We keep here the same notation used in Section 1 for identifying the sample orientation in the RD–ND (i.e. L, TB45, TB60 and TC). Henceforth, we will use the reference frame fixed to the sheet principal axes ($x_1 \equiv$ RD, $x_2 \equiv$ TD, $x_3 \equiv$ ND).

The first two examples show the influence of grain morphology: random aggregate with spherical and flat grains. Next three cases show the effect of the different texture components: $\{112\}\langle 11\bar{1}\rangle$ copper component, $\{110\}\langle 1\bar{1}2\rangle$ brass component and $\{001\}\langle 010\rangle$ cube component. Finally, we show a brass-type rolling texture with flat grains and recrystallization texture with spherical grains. The effect of each texture component is analyzed using a set of orientations

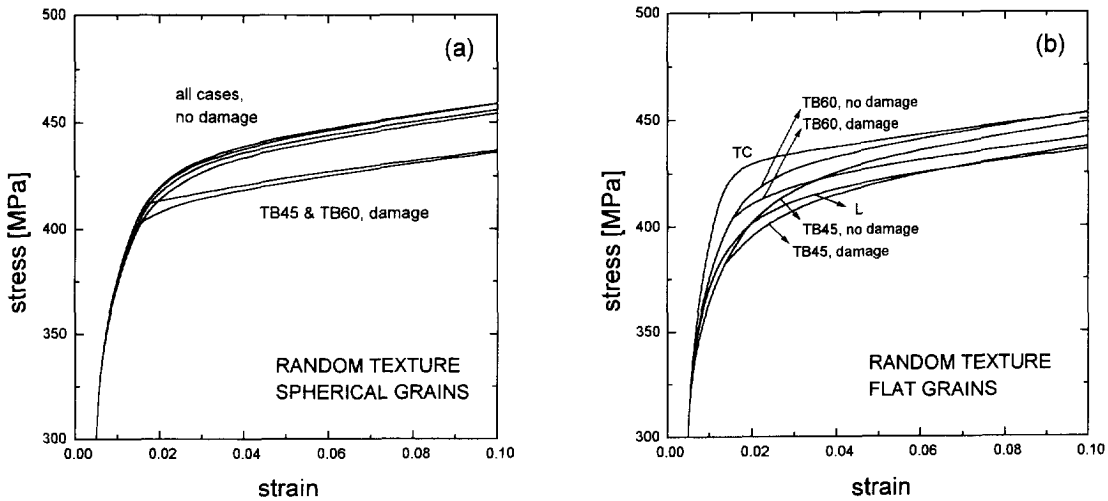

Fig. 2. Predicted stress–strain curves for random texture assuming: (a) spherical grains, (b) flat grains.

generated around each ideal orientation. On the other hand, the "rolling" texture consists of 50% of brass component, 25% of copper component and 25% of a random background, while the "recrystallization" texture consists of 60% of cube component and 40% of random background. The "rolling" texture is in good qualitative agreement with the one corresponding to the Al–Zn–Mg sample from where the experimental data displayed in Fig. 1 were obtained [4].

Some input data are kept fixed for all the cases, namely: the material is elastically isotropic ($\mu = 25$ GPa and $\nu = 0.4$), $\{111\}\langle 1\bar{1}0\rangle$ is the active slip mode with an initial $\tau^c = 150$ MPa. The microscopic hardening is assumed to be isotropic: each element of the hardening matrix $h^{ss'}$ [see equation (5)] is set to 30 MPa ($0.2\tau^c$). In the case of flat grains, the principal axes of the grain are aligned with the principal directions of the sheet. The relation between them is 1:0.75:0.1 (RD:TD:ND).

In what concerns modelling of damage, we adopt the following criteria based on the microstructural observations discussed in Section 2: a set of voids is "created" inside the material when either one of the following critical conditions are fulfilled

$$\Sigma_{33} = \Sigma^{cr} \tag{31}$$

$$E_{13} = \pm E^{cr} \tag{32}$$

where Σ_{33} and E_{13} are components of the current macroscopic Cauchy stress and strain tensors in sheet principal axes, respectively, while Σ^{cr} and E^{cr} are critical shear strain and opening stress for void nucleation. The assumed values for these critical parameters are $\Sigma^{cr} = 480$ MPa and $E^{cr} = 1\%$. The principal axes of the voids are initially aligned with the principal directions of the sheet but they are flatter than the grains: the aspect ratio is 1:0.75:0.01. The initial volume fraction of cavities amounts to 1% of the whole aggregate. Finally, it must be emphasized that all simulations were carried out switching on (label "damage") and off (label "no damage") the void creation criteria.

To start with, we discuss each case showing the calculated stress–strain curves and/or some statistical output of the simulations. Next, we compare the dependence of yield stress and bifurcation strain with the sample orientation predicted by the model with the experimental data displayed in Section 1. Finally, we investigate the sensitivity of the model to changes in the critical parameters for void nucleation.

Figure 2 shows the stress–strain curves (up to 10% true strain) corresponding to random texture with spherical and flat grains. Due to isotropy of texture and grain morphology, the "no damage" curves [Fig. 2(a)] for all orientations almost coincide. On the other hand, it is clear that the appearance of damage contributes to lowering the macroscopic hardening (this effect is observed for any kind of texture and grain shape considered). Concerning the "damage" cases, the critical condition equation (32) is reached in the TB45 and TB60 simulations but—due to the tensile sample orientation with respect to the sheet—this shearing condition will be never fulfilled in the TC and L cases. On the other hand, when pulling in the normal direction (TC orientation), the critical opening condition [equation (31)] is reached when the accumulated strain is greater than 10% so the effect of damage cannot be appreciated in the TC curve.

Figure 2(b) shows the case of a random aggregate with flat grains. If we compare the "no damage" curves with those in Fig. 2(a), it is evident that the grain shape anisotropy is responsible for some spread in the curves whence the predicted yield stresses and macroscopic hardening are slightly different from one sample orientation to another. This spread makes evident some differences in the microscopic states. In fact, all the different configurations of microscopic stress rates and strain rates are linked with the corresponding macroscopic state through equations (15) and (16) but the orientation of the tensile axis with respect to the

grain principal axes determines how much the local magnitudes deviate with respect to the average macroscopic magnitudes. Figure 3 shows the comparison between standard deviations (SD) in some stress rates and strain rates components (as a function of strain) for spherical and flat grains in the TC orientation. Some general features of these curves are: (1) As elastic isotropy is assumed, all stress and strain components are homogeneous up to approx. 0.5%. Heterogeneities start when the easiest slip system in the best orientated grain is activated. (2) Standard deviations increase during the elastoplastic transition and up to approx. 2%. Henceforth, they decrease and tend to stable values. When there is no grain shape effect, the model predicts higher deviations in stress than in strain, keeping close to the upper-bound limit. This feature is completely altered when grain shape effect is taken into account. In this case, shear strain rate $\dot{\epsilon}_{13}$ becomes severely heterogeneous while the normal stress rate in the loading direction ($\dot{\sigma}_{33}$) remains almost homogeneous, even during the elastoplastic transition.

The appearance of voids has a strong influence on the statistics. Figure 4 shows the SD of some components of stress rate and strain rate obtained in the "damage" and "no damage" cases for a random texture with spherical grains in the TB45 orientation. When voids are created, SD in strain rate components suddenly increases (especially for $\dot{\epsilon}_{33}$, the normal component in the "short" direction of the grains) while SD in stress rate decrease. These drops in SD make evident a high difference between the instantaneous response of new and pre-existing "particles": voids deform faster than grains and the local stresses associated with voids remain equal to zero throughout the calculation. Nevertheless, as deformation proceeds, it can be seen that the strain rate deviations in the "damage" case tend to decrease reaching stable values similar to those calculated in the "no damage" case. This tendency shows that the differences between strain rates of voids and grains decrease when the material reaches its stable fully plastic regime.

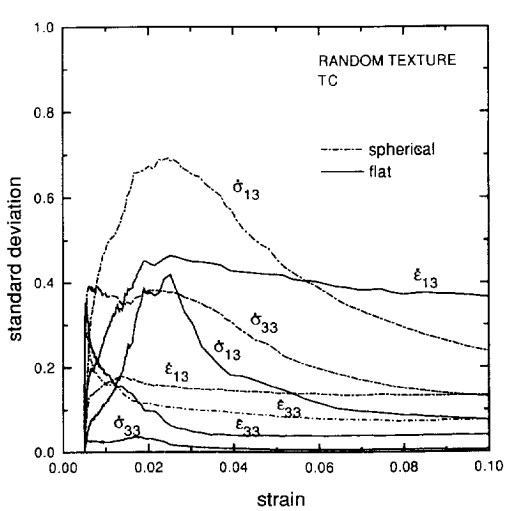

Fig. 3. Standard deviations of normal and shear stress rate and strain rate components. Random texture, TC orientation. Comparison between spherical and flat grains.

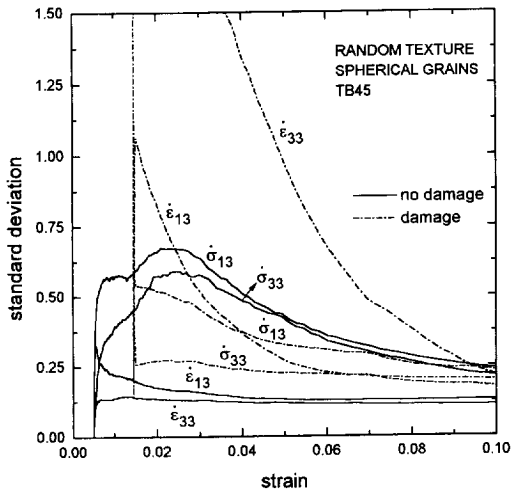

Fig. 4. Standard deviations of normal and shear stress rate and strain rate components. Random texture, TB45 sample. Comparison between "no damage" and "damage" cases.

Figure 5 shows the strain–stress curves for the copper, brass and cube components. Some interesting features displayed in these curves are:

(a) Great differences in yield stresses and macroscopic hardening appear between each case and each sample orientation. The predicted yield stress depends on the relative orientation with respect to the tensile direction of the available slip systems of a single crystal located in the ideal orientation. For example, in the "copper" case, when pulling in the RD direction (L curve), the tensile axis coincides with the $\langle 111 \rangle$ direction of a crystal in the ideal orientation. For such a crystal, the orientation factor ($1/m$) of the most heavily loaded slip systems (there are six slip systems in that condition) is very low (i.e. $1/m = 0.2725$). Whereas the actual set of orientations is built with a little spread around the ideal orientation, the yield condition is reached for a very high applied stress.

(b) The macroscopic hardening for the TB45 and TB60 orientations is significantly higher in the "brass" case than in the "copper" and "cube" cases, even when the assumed microscopic hardening is the same for the three cases. Therefore, this difference in the macroscopic behavior is a pure texture-induced effect.

(c) In the "brass" case for the TC sample orientation the macroscopic stress level is high enough to fulfill the critical condition (31) for an accumulated strain less that 10%. Hence, as for the TB cases, for a certain strain the initial single TC curve splits into the "damage" and "no damage" curves.

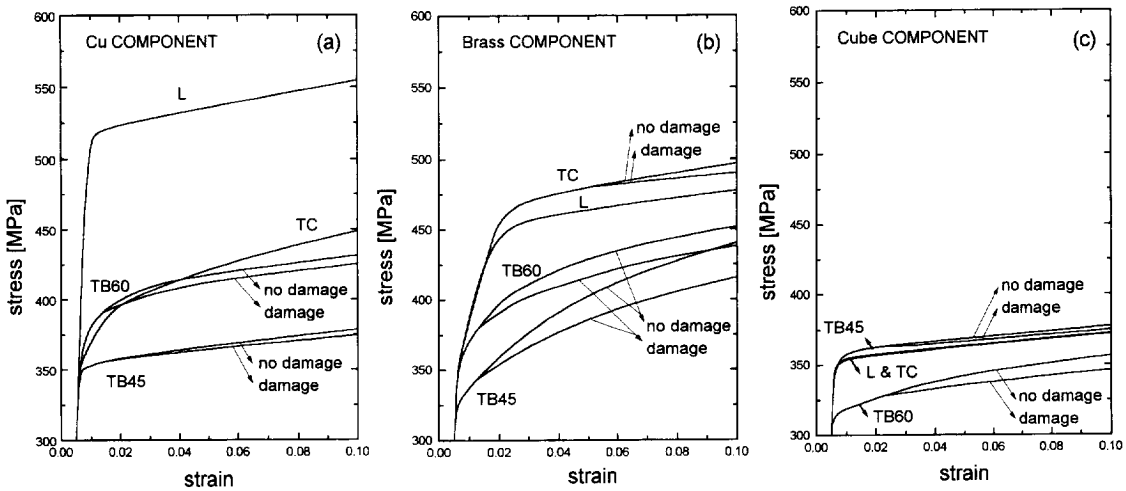

Fig. 5. Predicted stress–strain curves for different components: (a) copper, (b) brass, (c) cube.

(d) The L and TC curves for the "cube" case coincide due to the invariance of this texture component with respect to an interchange of the RD and ND direction.

Figure 6 displays the strain–stress curves calculated for rolling and recrystallization textures. The curves resemble those from their predominant component, namely: "rolling" and "recrystallization" curves are similar to "brass" and "cube" curves, respectively. However, as will be seen immediately, some differences appear in the predicted yield stresses and bifurcation strains due to the effect of the isotropic background of these textures.

Figure 7(a) shows—for all the previous cases—how the predicted yield stresses (0.2% plastic strain criterion) depend on the sample orientation. Likewise, Fig. 7(b) displays the orientation dependence of the bifurcation strains obtained in the "damage" cases while Table 1 shows the same for the "no damage" calculations. Caution should be taken in interpreting the ductility (>30) reported for some cases in Table 1, since a small strain theory is used to predict it. Those results should then be understood qualitatively as *large ductility*. Regarding the yield stress curves it can be seen that:

(a) As it was stated previously, there is no dependence of the yield stress with the sample orientation in the fully isotropic case. The flat grain shape determines that $\sigma_y(L) < \sigma_y(TC)$. Due to high SD in stress rates in the L case some grains reach the microyielding condition for a lower macroscopic stress level than in the TC case. Hence, in the former case, whereas the accumulated plastic strain grows faster, the 0.2% plastic strain (e.g. the macroyielding condition) is reached earlier than in the latter case.

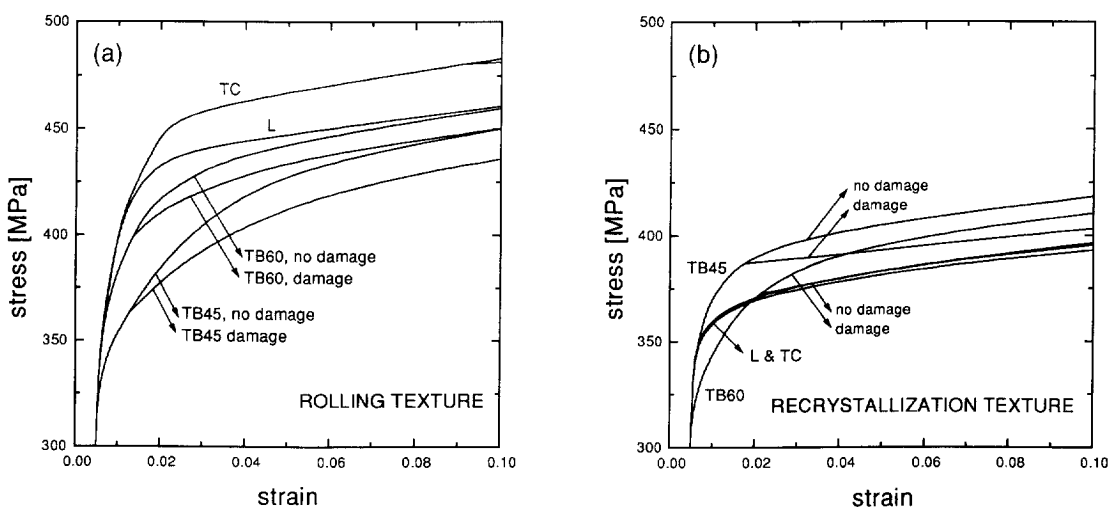

Fig. 6. Predicted stress–strain curves for different textures: (a) rolling, (b) recrystallization.

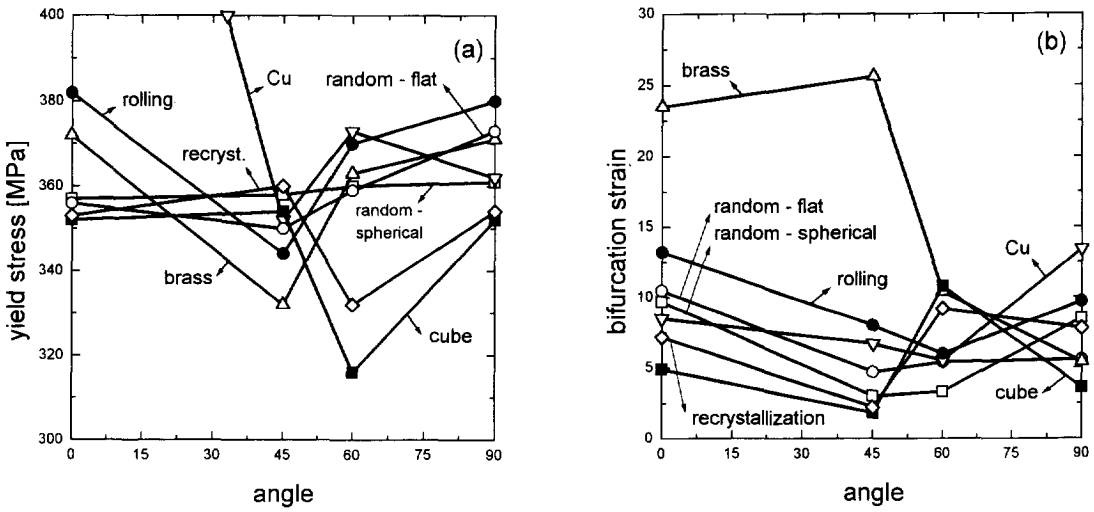

Fig. 7. Predicted yield stress and ductility profiles.

(b) One of the mean features of the yield stress profile of the Al–Zn–Mg sheets reported by Solas *et al.* [4], (i.e. a high yield stress for the L sample compared with other orientations, see Fig. 1) is well reproduced in the "rolling" case. Therefore, this kind of orientation dependence would be mainly a texture-induced effect.

(c) The highest and lowest yield stresses are predicted in the "copper" case for the L orientation and in the "cube" case for TB60 orientation, respectively. Both extremes are determined by the relative orientation of the tensile direction and the available slip systems of the crystalline ideal orientation.

Concerning the predicted bifurcation strains [Fig. 7(b) and Table 1] we conclude that:

(a) In general, when the damage mechanisms are taken into account, lower bifurcation strains are predicted. Evidently, this effect is linked with the lowering of macroscopic hardening obtained in the "damage" cases.

(b) Except in the "cube" and "recrystallization" cases the minimum in ductility predicted for the TB orientations is an effect closely related with damage modelling. Otherwise, for the "no damage" simulations, the TB45 and TB60 are more stable than the TC and L orientations.

(c) The "brass" case is quite stable. Nevertheless, due to the addition of the copper component and the isotropic background to give the rolling texture, the predicted bifurcation strains are severely lowered.

(d) The predicted dependence of ductility with the sample orientation for the "rolling" case is in good qualitative agreement with the reported Al–Zn–Mg sheet ductility profile (see Fig. 1).

(e) The "cube" component and, hence, the "recrystallization" texture are quite instable cases due to a low predicted macroscopic hardening except for the TB60 simulation, where a low macroscopic stress level determines a higher ductility for this orientation.

Table 1. Bifurcation strains obtained for the "no damage" calculations

Case	L	TB45	TB60	TC
Random–spherical	9.7	9.6	10.2	8.5
Random–flat	10.5	13.6	10.3	5.6
Copper	8.5	>30	>30	13.4
Brass	>30	>30	>30	>30
Cube	4.9	1.8	14.2	3.6
Rolling	13.2	>30	>30	>30
Recrystallization	7.2	4.3	9.2	7.8

Finally, we show how the selection of different critical parameters for void nucleation affects the results of our simulations. Figure 8 shows the way in which the changes of the critical parameters affect the predicted ductility profile for the random texture, flat grains case. For different opening stresses, the only point affected is the one corresponding to the TC simulation. The bifurcation strain predicted for this orientation diminishes as the critical opening stress diminishes. On the other hand, whereas the nucleation of voids by shearing needs higher level of shear strain, the TB points are lifted. Therefore, when shearing damage is not an available mechanism, the ductility profile shows a maximum for the TB orientations.

5. CONCLUSIONS

The damage nucleation in Al–Zn–Mg alloys takes place at grain boundaries, where hard particles act as stress concentrators and cavity generators. Eventually, during testing these cavities will coalesce leading to fracture. The yield stress and ductility profiles of these alloys after large rolling deformations need to be understood and predicted.

An elastoplastic self-consistent model has been developed in which the constituent elements are the

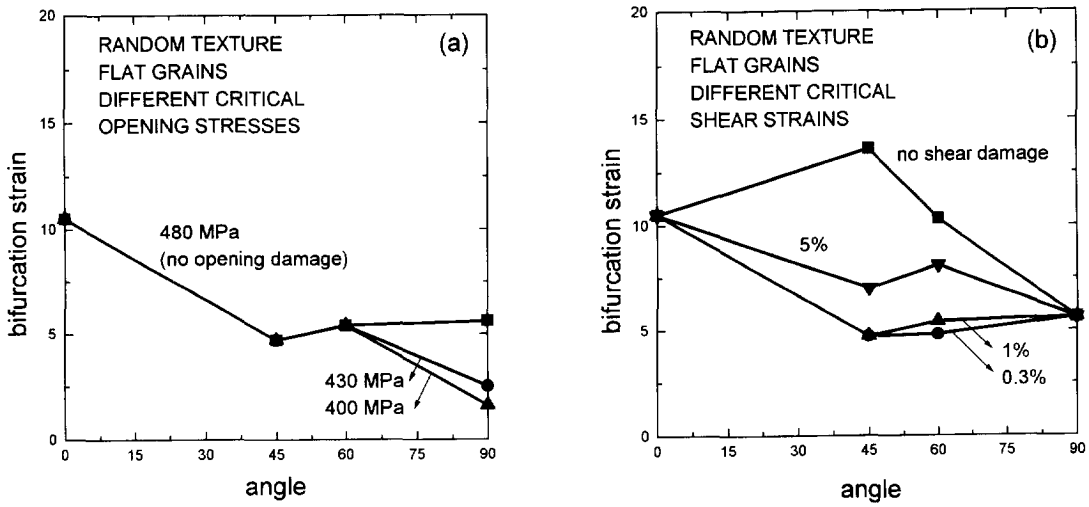

Fig. 8. Predicted ductility profiles for different critical parameters.

grains, with their crystalline orientation and morphology, and the voids formed at the grain boundary. Both grain and void shapes (and volume) are updated, allowing the evolution of damage to be followed, and enabling us to derive the macroscopic behavior. From this approach the stress–strain curves and therefore the yield stresses are obtained.

A bifurcation analysis for compressible anisotropic solids has been developed leading to an estimation of the ductility.

The model was applied for the cases of different well known textures, and it is shown that the texture has a dramatic influence on the predicted results.

It has also been applied for different grain shapes showing a marked effect.

Typical yield stress and ductility profiles as a function of the tensile angle could be predicted in good qualitative agreement with the observed profiles. A real comparison would necessitate a good knowledge of the texture, grain shapes and the critical parameters controlling the damage initiation.

Acknowledgement—One of the authors (R.L.) wishes to acknowledge CNRS-PIRMAT for financial support during his four months stay at GPM2 as Research Associate.

REFERENCES

1. R. Hill, *The Mathematical Theory of Plasticity*. Oxford University Press, London (1950).
2. T. Kawabata and O. Izumi, *Acta metall.* **24,** 817 (1976).
3. J. D. Embury and E. Nes, *Z. Metallk.* **65,** 45 (1974).
4. D. Solas, Y. Brechet, F. Louchet and J.C. Ehrstrohm, *Mater. Sci. Engng*. Submitted.
5. A. K. Vasudevan and R. D. Doherty, *Acta metall.* **38,** 1193 (1987).
6. R. Hill, *J. Mech. Phys. Solids* **13,** 89 (1965).
7. J. W. Hutchinson, *Proc. R. Soc. Lond. A* **319,** 247 (1970).
8. R. Hill, *J. Mech. Phys. Solids* **6,** 236 (1958).
9. R. Hill and J.W. Hutchinson, *J. Mech. Phys. Solids* **23,** 239 (1975).
10. S. Stören and J. R. Rice, *J. Mech. Phys. Solids* **23,** 421 (1975).
11. J. W. Hutchinson and K. W. Neale, in *Mechanics of Sheet Metal Forming* (edited by D. P. Koistinen and N. M. Wang), p. 127. Plenum Press, New York (1978).
12. J. D. Eshelby, *Proc. Roy. S. Lond. A* **241,** 376 (1957).
13. R. A. Lebensohn and C. N. Tomé, *Phil. Mag. A* **67,** 187 (1993).
14. L. J. Walpole, *J. Mech. Phys. Solids* **17,** 235 (1969).
15. S. Nemat-Nasser and M. Obata, *Proc. Roy. S. Lond. A* **407,** 343 (1986).
16. R. A. Lebensohn and C.N. Tomé, *Acta metall. mater.* **41,** 2611 (1993).
17. G. R. Canova, U. F. Kocks, C. Fressengeas, D. Dudzinski, Ph. Lequeu and G. Sornberger, *Proc. ICOTOM* 8 (edited by J. S. Kallend and G. Gottstein), Santa Fe (1988).
18. G. R. Canova, U. F. Kocks, C. N. Tomé and J. J. Jonas, *J Mech. Phys. Solids* **33,** 371 (1985).

APPENDIX

For convenience, it has been chosen to use a "vector" notation for tensors in the following way. Any second rank symmetric tensor **r**, is transformed into the vector

$$\mathbf{r} = [r_{11}, r_{22}, r_{33}, r_{23}\sqrt{2}, r_{13}\sqrt{2}, r_{12}\sqrt{2}]. \tag{A1}$$

The material has in its state prior to tensile testing, an orthotropic symmetry, with respect to the sheet principal axes, but looses at least partially this particular symmetry during tension. The tensile samples have their flat surface coincident with the transverse plane (i.e. normal to TD) and the tensile axis X_3 lies between ND and RD. Calling X_2 the axis in TD, the remaining symmetry of the material, after tensile testing, is so that the stress subspace $\{\sigma_{11}, \sigma_{22}, \sigma_{33}, \sigma_{13}\}$ is "closed", as well as the subspaces $\{\sigma_{23}\}$ and $\{\sigma_{12}\}$. This means, after Canova *et al.* [18], that any stress state lying inside the first subspace will produce a strain rate not necessarily colinear to it, but also included in that same subspace. In particular, a pure tensile stress may induce tensile strain rate together with shearing $\dot{\epsilon}_{13}$. The same applies to the other subspaces, and, in particular, a stress σ_{23} will only induce a shear rate $\dot{\epsilon}_{23}$. It can be simply deduced that in the (X_1, X_2, X_3) reference system the tangent tensor **L** must be of the form

$$\begin{matrix} L_{11} & L_{12} & L_{13} & 0 & L_{15} & 0 \\ L_{12} & L_{22} & L_{23} & 0 & L_{25} & 0 \\ L_{13} & L_{23} & L_{33} & 0 & L_{35} & 0 \\ 0 & 0 & 0 & L_{44} & 0 & 0 \\ L_{15} & L_{25} & L_{35} & 0 & L_{55} & 0 \\ 0 & 0 & 0 & 0 & 0 & L_{66} \end{matrix} \tag{A2}$$

where the necessary intrinsic symmetry of **L** has been used.

The jumps in the rate of volume changes are expressed by the equations

$$\Delta\mathrm{tr}(\dot{\epsilon}) = (1 - 2\nu)\frac{\Delta\mathrm{tr}(\dot{\sigma})}{2\mu(1+\nu)} = K\frac{\Delta\dot{p}}{2\mu} \tag{A3}$$

which can be written as

$$\Delta\mathrm{tr}(\dot{\epsilon}) = \alpha_1\Delta\dot{\epsilon}_1 + \alpha_3\Delta\dot{\epsilon}_3 + \alpha_5\Delta\dot{\epsilon}_5 \tag{A4}$$

with the α_i coefficients defined by

$$\begin{aligned}\alpha_1 &= F(L_{11} + L_{31} - L_{12} - L_{32})\\ \alpha_3 &= F(L_{33} + L_{13} - L_{12} - L_{32})\\ \alpha_5 &= \frac{1}{\sqrt{2}}F(L_{15} + L_{35})\end{aligned} \tag{A5}$$

with

$$F = \frac{K}{(6\mu - K[L_{12} + L_{32}])}. \tag{A6}$$

All the terms in equation (A5) are equal to zero for an incompressible material.

The jumps in the useful components of the nominal stress rate can be expressed as

$$\begin{aligned}\Delta\dot{t}_{11} &= H_{11}\Delta\dot{\epsilon}_1 + H_{13}\Delta\dot{\epsilon}_3 + H_{15}\Delta\dot{\epsilon}_5\\ \Delta\dot{t}_{31} &= H_{51}\Delta\dot{\epsilon}_1 + H_{53}\Delta\dot{\epsilon}_3 + H_{55}\Delta\dot{\epsilon}_5\\ \Delta\dot{t}_{33} &= H_{31}\Delta\dot{\epsilon}_1 + H_{33}\Delta\dot{\epsilon}_3 + H_{35}\Delta\dot{\epsilon}_5\\ \Delta\dot{t}_{13} &= \Delta\dot{t}_{31} - g_1 n_3\sigma_3\end{aligned} \tag{A7}$$

with the H coefficients defined by

$$\begin{aligned}H_{11} &= L_{11} - L_{12} + \alpha_1 L_{12}\\ H_{13} &= L_{13} - L_{12} + \alpha_3 L_{12}\\ H_{15} &= L_{15} + \alpha_5\\ H_{51} &= \frac{1}{\sqrt{2}}(L_{51} - L_{52} + \alpha_1 L_{52})\\ H_{53} &= \frac{1}{\sqrt{2}}(L_{53} - L_{52} + \alpha_3 L_{52})\\ H_{55} &= (L_{55} + \alpha_5 L_{52})\\ H_{31} &= L_{31} - L_{32} + \alpha_1[L_{32} + \sigma_3]\\ H_{33} &= L_{33} - L_{32} - \sigma_3 + \alpha_3[L_{32} + \sigma_3]\\ H_{35} &= L_{35} + \alpha_5[L_{32} + \sigma_3]\end{aligned} \tag{A8}$$

Defining the quantity $\chi = n_1/n_3$ and using equation (A7) in equation (28), the linear system expressed in equation (30) can be written as

$$\begin{vmatrix} A & B \\ C & D \end{vmatrix} \times \begin{vmatrix} g_1 \\ g_3 \end{vmatrix} = \begin{vmatrix} 0 \\ 0 \end{vmatrix} \tag{A9}$$

where

$$\begin{aligned}A &= H_{11}\chi^2 + \chi(H_{15} + H_{51}) + H_{55}\\ B &= \chi^2 H_{15} + \chi(H_{13} + H_{55}) + H_{53}\\ C &= H_{51}\chi^2 + \chi(H_{55} + H_{31} - \sigma_3) + H_{35}\\ D &= \chi^2 H_{55} + \chi(H_{53} + H_{35}) + H_{33}.\end{aligned} \tag{A10}$$